ACS NANO

www.acsnano.org

ARTICLE

Isomer Discrimination via Defect Engineering in Monolayer MoS_2

Bin Han, Sai Manoj Gali, Shuting Dai, David Beljonne, and Paolo Samorì*

Cite This: *ACS Nano* 2023, 17, 17956–17965

Read Online

ACCESS | Metrics & More | Article Recommendations | Supporting Information

ABSTRACT: The all-surface nature of two-dimensional (2D) materials renders them highly sensitive to environmental changes, enabling the on-demand tailoring of their physical properties. Transition metal dichalcogenides, such as 2H molybdenum disulfide (MoS_2), can be used as a sensory material capable of discriminating molecules possessing a similar structure with a high sensitivity. Among them, the identification of isomers represents an unexplored and challenging case. Here, we demonstrate that chemical functionalization of defect-engineered monolayer MoS_2 enables isomer discrimination via a field-effect transistor readout. A multiscale characterization comprising X-ray photoelectron spectroscopy, Raman spectroscopy, photoluminescence spectroscopy, and electrical measurement corroborated by theoretical calculations revealed that monolayer MoS_2 exhibits exceptional sensitivity to the differences in the dipolar nature of molecules arising from their chemical structure such as the one in difluorobenzenethiol isomers, allowing their precise recognition. Our findings underscore the potential of 2D materials for molecular discrimination purposes, in particular for the identification of complex isomers.

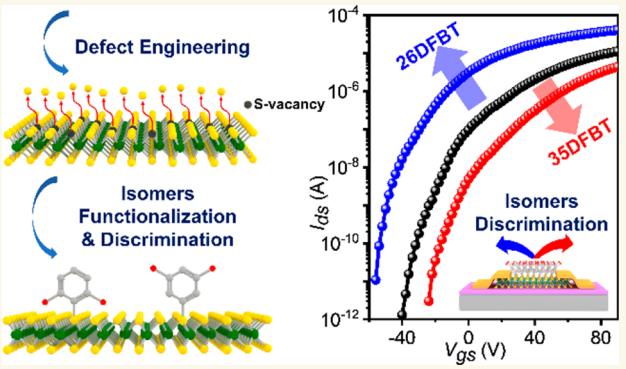

KEYWORDS: *2D materials, MoS_2, defect engineering, molecular functionalization, isomer discrimination*

Over the past decade, two-dimensional (2D) transition metal dichalcogenides (TMDCs) have captured significant attention due to their exceptional electronic, optical, and mechanical properties.[1−4] Among them, molybdenum disulfide (MoS_2) has emerged as a highly promising material for next-generation (opto-)electronic devices due to its exceptional characteristics, including high electron mobility, high I_{on}/I_{off} ratio, tunable bandgap (from an indirect bandgap of bulk material to a direct bandgap of a monolayer), and strong light−matter interactions.[5−7] Furthermore, the weak interlayer interactions, dangling-bond-free atomically flat surfaces, and van der Waals bonding between adjacent layers of MoS_2 make it an ideal platform for developing atomically thin devices, such as photodetectors, photodiodes, and heterojunction devices.[8,9]

The combination with organic molecules has been proven to be an effective method to adjust the properties of MoS_2 via doping as a route to impart responsiveness to optical stimuli and chemical sensing capabilities as well as for realizing complementary metal−oxide−semiconductor circuits.[10−12] Defects in MoS_2 crystals are extremely reactive sites for the chemisorption of molecules enabling the generation of strong chemical bonds between MoS_2 and organic compounds. This method has several advantages, such as the protocol's simplicity, controllable number of bonded molecules, and higher stability compared with van der Waals interaction of physical adsorption. These advantages have rendered chemisorption an attractive approach for exploring the effect of molecular functionalization of MoS_2 by developing *ad-hoc* functions for various applications.

Unfortunately, mechanically exfoliated MoS_2 crystals exhibit very few defects (defect concentration <2%), making them inappropriate for chemical bonding with molecules.[13,14] Conversely, chemically vapor-deposited (CVD, defect concentration ≲3%)[15,16] or chemically (liquid) exfoliated MoS_2 (defect concentration >3%)[17,18] are more suitable for chemisorption strategies, but their excessively abundant defects and traps, disordered structure, and inevitable ion residues lead to lower carrier mobility, lower I_{on}/I_{off} ratios, and overall poorer device performance, ultimately limiting their application in optoelectronic devices.[19−21] To overcome this problem,

Received: May 10, 2023
Accepted: September 8, 2023
Published: September 13, 2023

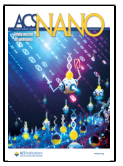

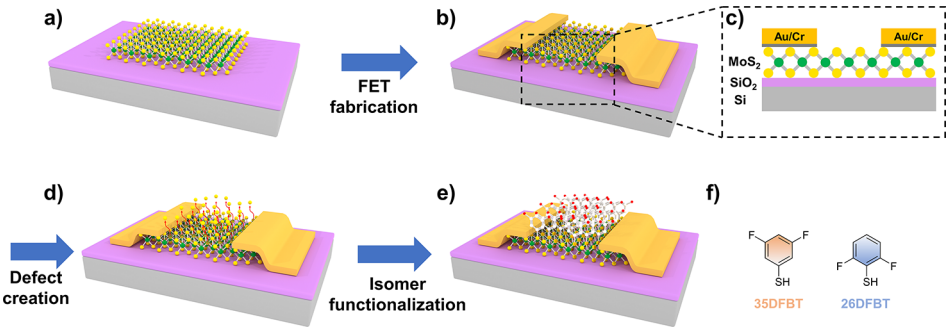

Figure 1. Schematic illustration of the preparation steps for the isomer-functionalized FETs. (a) Exfoliated monolayer MoS_2 flake on the SiO_2/Si substrate. (b) FET device fabricated by photolithography. (c) Cross-sectional view of FETs. (d) Defects induced on the surface of monolayer MoS_2 through defect engineering. (e) Functionalization of a monolayer MoS_2 semiconductor with isomers via molecular grafting. (f) Chemical structure of the isomers (35DFBT and 26DFBT).

defect engineering has been proposed as a strategy to create defects on the surface of TMDCs to tailor their properties and enable device chemical functionalization.[22] According to theoretical studies, the Mo−S bond has the lowest stability within the structure. When subjected to an external etching source, the Mo−S bond will break, allowing sulfur atoms to escape from the surface.[23,24] Several approaches have been reported for modulating the defect density of chalcogen vacancies, including high-temperature thermal annealing,[25,26] ion irradiation/bombardment,[13,25,27] electron irradiation,[28] and plasma treatments.[29,30] These defects can function as active sites for the hydrogen evolution reaction (HER), improving the catalytic activity of MoS_2 in HER.[31] Importantly, the controlled generation of defects in the MoS_2 nanosheets does not irreversibly damage their crystal structure: defect healing via molecular functionalization makes it possible to recover the material's electronic and optical properties.[11,32,33] In fact, these chalcogenide vacancies serve as anchoring sites for surface functionalization, which can enable covalent grafting of thiolated molecules, yielding a modulation of the chemical, vibrational, electronic, optical, and magnetic properties of the 2D crystals.[22,34] The high sensitivity of defect-containing TMDCs to their environment implies that even subtle modifications on their surface can significantly influence their intrinsic properties, rendering them highly sensitive for the identification of simple or complex, yet similar molecules, potentially including isomers. The latter is highly sought after because the very similar properties of isomers make their discrimination unattainable with conventional discrimination methods.[35] However, despite this potential, the dearth of reports on isomer recognition by TMDCs in the literature underscores a promising area for future research and development.

Here, we explore the application of defect engineering in monolayer MoS_2 for isomer discrimination. We exposed field-effect transistors (FETs) based on mechanically exfoliated monolayer MoS_2 to a high-temperature treatment to create S-vacancy defects in the channel region. The devices were then chemically functionalized with thiolated difluorobenzenethiol isomers to enable their identification. To gain an exhaustive insight and control over this functionalization process, we performed a comprehensive multiscale experimental and theoretical investigation on the optical, optoelectronic, and electrical properties of MoS_2 before and after molecular functionalization.

RESULTS AND DISCUSSION

The sample preparation protocol is illustrated in Figure 1. Monolayer MoS_2 flakes were mechanically exfoliated on a heavily doped silicon substrate capped by a 270-nm-thick thermally grown SiO_2 dielectric layer. The monolayer thick flakes were identified by optical microscopy with photoluminescence (PL) and confirmed by Raman spectroscopy and atomic force microscopy (AFM), the latter exhibiting a thickness of about 0.80 nm, consistent with previous reports (see optical micrograph and corresponding AFM height image in Figure S1 in the Supporting Information).[36] Back-gate MoS_2 FETs were then fabricated using conventional photolithography and lift-off processes, and the electrodes were deposited with 0.2 nm of Cr as an adhesion layer and 60 nm Au. To generate sulfur-vacancy (S-vacancy) defects, the device samples were exposed to 300 °C for 1 h. Then, the defective MoS_2 (d-MoS_2) sample was functionalized with thiolated molecules. Details of the experimental protocol can be found in the Experimental Section. In particular, as prototypical systems, we have selected two isomers of difluorobenzenethiol, i.e., 2,6-difluorobenzenethiol (26DFBT) and 3,5-difluorobenzenethiol (35DFBT), possessing identical chemical formulas but different dipole moment orientation. Figure 1f depicts the chemical structures of these two isomers. Upon MoS_2 functionalization, the different arrangement of F atoms in these molecules determines a dissimilar dipole moment orientation, resulting in distinct dipole-induced electrostatic gating manipulating the carrier density of the underlying 2D semiconductor.[37,38] This provides a tool for isomer discrimination, which can be confirmed by the difference in secondary-electron cutoff, as shown in Figure S3. Our methodology combines a variety of significant advantages. First, we employ a monolayer MoS_2 crystal, which provides a notably more sensitive surface than few-layer or multilayer thick crystals. Second, high-temperature treatment was conducted in a glovebox filled with inert gas in order to prevent extensive deterioration of monolayer MoS_2 crystals in the presence of air. Third, in lieu of using traditional molecular modification techniques such as physical adsorption, vapor deposition, and molecular coordination, we choose a chemically more controlled and robust solution based on the direct formation of covalent bonds between molecules and MoS_2 crystals. Fourth, compared with previous works on molecular doping, we utilize structurally similar isomers whose dipole differences enable discrimination. The devised approach based on the TMDCs' controlled functionalization for the identi-

https://doi.org/10.1021/acsnano.3c04194
ACS Nano 2023, 17, 17956−17965

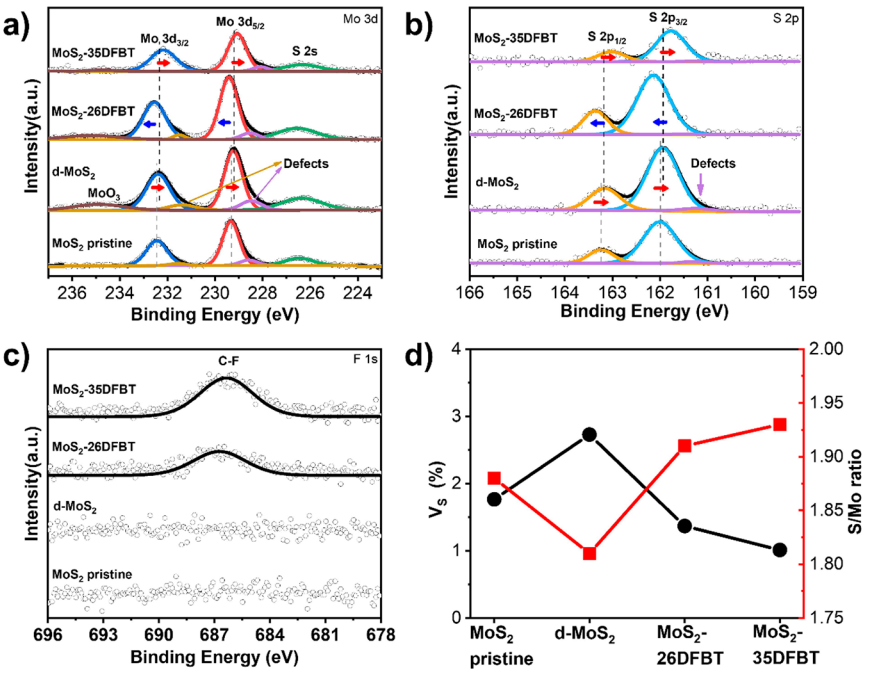

Figure 2. (a–c) High-resolution XPS Mo 3d, S 2p, and F 1s core-level spectra of isomer-functionalized MoS_2 compared to the corresponding pristine and defect-induced surface. (d) Sulfur vacancy concentration (V_S) and S/Mo stoichiometric ratio of different samples.

fication of isomers is universal. Last, the combined optical, optoelectronic, and electrical characterization and theoretical calculations provide an exhaustive and clear evidence of the dipole-induced doping effects brought about by the covalent modification of isomers, representing a notable advancement in TMDC functionalization for molecular identification purposes.

The morphology and electronic structure of the MoS_2 monolayer crystal at each step of the process were assessed *in situ* to detect changes and confirm the covalent grafting of the molecular isomers onto the basal plane of MoS_2. Figure S2a,d show the optical microscopy images of monolayer MoS_2, while Figure S1 displays the AFM topographical image. The pristine monolayer MoS_2 crystal exhibits an atomically flat surface with a root-mean-square roughness (R_{RMS}) of approximately 0.5 nm, due to its easy-to-peel van der Waals layered structure and the absence of dangling bonds on the surface.[39,40] Figure S2b and e confirm the absence of changes in the thickness and roughness of MoS_2 upon the introduction of defects. However, after molecular functionalization, a considerable increase in the average thickness of the MoS_2 monolayer has been observed. Figures S2c and f show that the thickness of monolayer MoS_2 augmented from 0.59 to 1.45 nm after the functionalization of 26DFBT molecules and from 0.66 to 1.46 nm after the modification of 35DFBT molecules. This increase in thickness can be ascribed to the covalent tethering of the difluorobenzenethiol molecules, as confirmed by the variation in vertical distance before and after functionalization, well matching the van der Waals contour of the grafted molecule. The thickness of 35DFBT is slightly higher than that of 26DFBT because the F atoms are oriented upward. In addition, after molecular grafting small grains appeared on the MoS_2 surface, and the R_{RMS} increased from 0.55 nm to 0.62 nm for the 26DFBT-functionalized sample and from 0.60 to 0.88 nm for the 35DFBT-functionalized sample, respectively, which is consistent with previous results.[41,42] The above findings provide clear evidence that the difluorobenzenethiol isomers were successfully grafted to the MoS_2 surface.

High-resolution X-ray photoelectron spectroscopy (XPS) analyses provide important insights for assessing changes in the electronic structure of monolayer MoS_2 before and after isomer functionalization. Figure 2 portrays the Mo 3d, S 2p, and F 1s core-level spectra of the MoS_2 monolayer for each step of the treatment. In the Mo 3d core energy level spectrum, the MoS_2 pristine monolayer shows spin–orbit splitting doublets from lattice Mo–S at 229.30 eV (Mo 3d 5/2, red curve) and 232.44 eV (Mo 3d 3/2, blue curve). Correspondingly, the S 2p core energy level spectrum exhibits spin–orbit splitting doublets at 162.01 eV (S 2p 3/2, cyan curve) and 163.23 eV (S 2p 1/2, beige curve).[43,44] Interestingly, two additional shoulder doublets appeared at slightly lower binding energies of the Mo 3d peak (purple curve at 228.50 eV and khaki curve at 231.5 eV), which can be attributed to vacancy neighboring atoms. This feature is due to the chemical reduction of Mo caused by a sulfur deficiency (valence of Mo < 4). Moreover, an additional component at the lower binding energy of 161.5 eV for S 2p was also attributed to S-vacancy defects.[15,43] The S-vacancy defect concentration (V_S, see Supporting Information for calculation details) and S/Mo stoichiometric ratio of MoS_2 were calculated from the integrated area of the S and Mo components. As shown in Figure 2d, the calculated V_S of mechanically exfoliated MoS_2 amounts to 1.77%, and the S/Mo stoichiometric ratio was 1:1.88, in line with previous results.[42] After high-temperature treatment, both Mo and S doublets shift toward lower binding energies, and the intensity of the defect component peaks increases notably, indicating that the Fermi level shifts toward the valence band (VB) edge.[44] Table S1 summarizes the shift amount of Mo 3d and S 2p peak positions before and after treatment. The V_S increased up to 2.73%, and the S/Mo ratio decreased to 1:1.81, indicating the increased defectiveness of the crystal, providing abundant sites for subsequent function-

https://doi.org/10.1021/acsnano.3c04194
ACS Nano 2023, 17, 17956–17965

alization. Interestingly, a weak deconvoluted peak appeared at higher binding energies (235 eV), which indicates the presence of oxidized molybdenum, suggesting partial oxidation of the Mo atoms.[45]

The F 1s core energy spectra of the isomer-functionalized samples are shown in Figure 2c. Both spectra exhibit a distinct single peak that originates from the C−F bond in the molecule. The 35DFBT-functionalized MoS_2 shows a higher intensity peak signal compared to the 26DFBT-modified sample due to the exposed double F atoms in its molecular structure, which confirms again the isomer functionalization on the MoS_2 surface. However, the Mo 3d and S 2s spectra of functionalized MoS_2 indicate a clear shift in opposite directions. Table 1 provides a summary of the amount of shift of the Mo 3d and S 2p peak positions before and after functionalization. The Mo and S peaks of MoS_2 shift toward higher binding energies by about 0.2 eV after functionalization with 26DFBT, indicating that the Fermi level was closer to the conduction band (CB) edge and corresponding to n-type electron doping. In contrast, upon functionalization with 35DFBT, both Mo and S peaks of MoS_2 shift toward lower binding energy by about 0.16 eV, suggesting the Fermi level was closer to the VB edge and corresponding to p-type hole doping.[46] No additional peak was detected near 164 eV in the S 2p spectrum, indicating the absence of free or unbound thiol, i.e., no physisorbed molecules on the MoS_2 surface.[47,48] After isomer modification, the V_S of MoS_2 significantly reduced to 1.37% and 1.01%, and the S/Mo ratio increased to 1:1.91 and 1:1.93, corresponding to the functionalization of 26DFBT and 35DFBT, respectively. The difference in V_S after isomer functionalization can be explained by the steric hindrance of the two fluorine substituents in 26DFBT for the chemisorption process, which results in a slightly lower surface coverage of 26DFBT molecules than that of 35DFBT molecules. These results suggest that thiol-containing isomers can graft onto the MoS_2 surface through covalent bonding and are capable of repairing the S-vacancy defects.[13,49,50]

Table 1. Shifts of Mo 3d and S 2p Peaks before and after Isomer Functionalization in XPS Results

	d-MoS_2 (eV)	MoS_2-26DFBT (eV)	Δ^a (eV)	MoS_2-35DFBT (eV)	Δ^a (eV)
Mo 3d 3/2	232.35	232.57	0.22	232.18	−0.17
Mo 3d 5/2	229.21	229.42	0.21	229.07	−0.14
S 2p1/2	163.17	163.34	0.17	163.02	−0.15
S 2p3/2	161.93	162.14	0.21	161.76	−0.17

$^a\Delta$ represents the difference with d-MoS_2.

To gain further insight into the impact of defects and isomeric functionalization on the electronic and optical properties of MoS_2 monolayers, Raman and PL spectra were recorded. The Raman spectra of a typical MoS_2 monolayer, featuring an in-plane E^1_{2g} vibrational mode of Mo and S atoms at ~386 cm^{-1} and an out-of-plane A_{1g} vibrational mode of the S atom at ~404.5 cm^{-1}, as shown in Figure 3a and b. The frequency difference between the two vibrational modes is layer dependent and is below 20 cm^{-1} for the monolayer (see Figure S4 for Raman spectra of monolayer MoS_2).[36,51] The defect-generating treatment resulted in a small blueshift in the

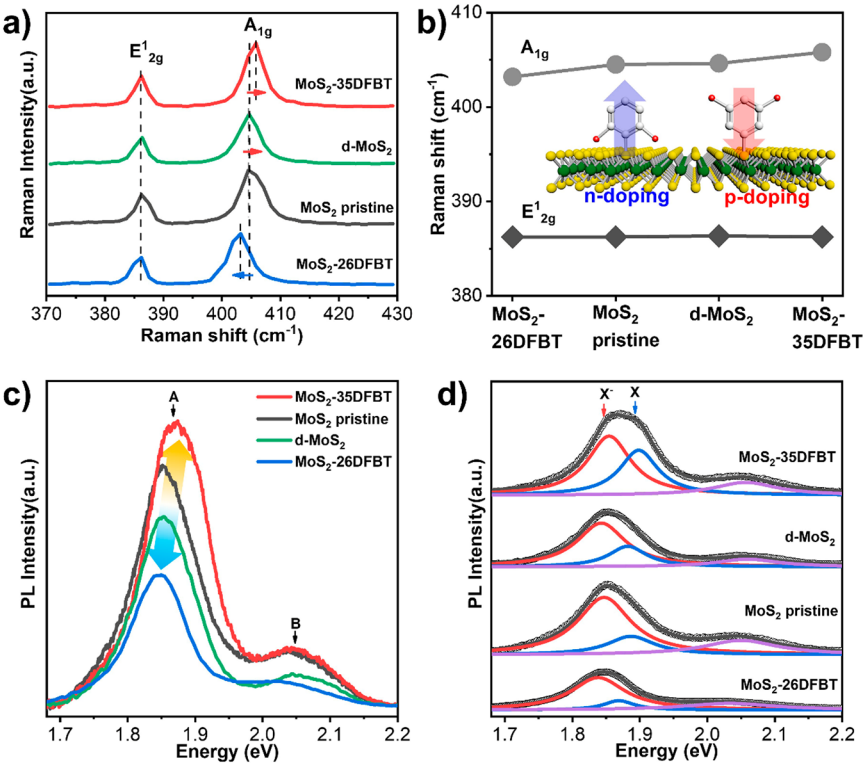

Figure 3. (a) Raman spectra of pristine MoS_2, d-MoS_2, and functionalized with isomers. (b) Plot of the Raman shift in E^1_{2g} mode and A_{1g} mode in (a). The inset demonstrates the dipole-induced doping effect and the dipole moment orientation of isomers functionalized on a MoS_2 monolayer. (c) PL spectra of pristine MoS_2, d-MoS_2, and functionalized with isomer. (d) Analysis of the PL spectra with peak deconvolution.

https://doi.org/10.1021/acsnano.3c04194
ACS Nano 2023, 17, 17956−17965

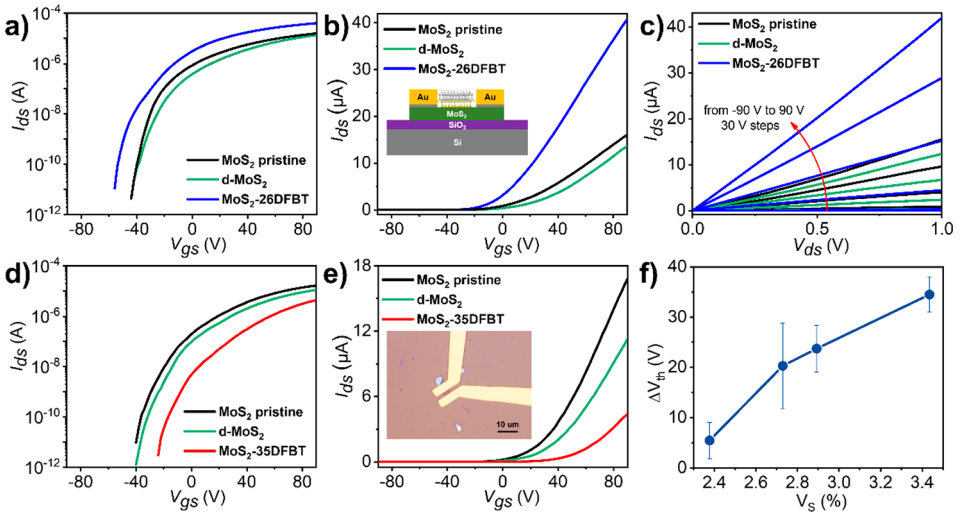

Figure 4. (a, b) Logarithmic and linear transfer curves (I_{ds}−V_{gs}) of pristine monolayer MoS_2 FETs, after induced defect and after functionalized with 26DFBT molecules. The applied bias is 1 V. The illustration in (b) is the schematic diagram of MoS_2 FETs functionalized with 26DFBT molecules. The channel length/width is 1.21 μm/4.65 μm. (c) Output curves (I_{ds}−V_{ds}) of the above devices. (d, e) Logarithmic and linear transfer curves (I_{ds}−V_{gs}) of pristine monolayer MoS_2 FETs, after induced defect and after functionalized with 35DFBT molecules. The applied bias is 1 V. The inset in (e) shows the optical microscopy image of the device based on the pristine MoS_2 monolayer. The channel length/width is 1.73 μm/2.59 μm. (f) Change of threshold voltage (ΔV_{th}) of the devices before and after 26DFBT functionalization at different V_S.

A_{1g} peak by 0.12 cm^{-1} (from the gray vertical dashed line to the black vertical dashed line in Figure 3a), and this offset correlated with the change in V_S (which increased by 0.96%), in agreement with defects induced by thermal annealing and ion irradiation.[13,52] However, after molecular functionalization, the A_{1g} peak shifts in two opposite directions compared to d-MoS_2 containing S-vacancy defects. It has been reported that the A_{1g} mode is more sensitive to charge changes within MoS_2 than E^1_{2g} and that a redshift of A_{1g} corresponds to higher electron concentration (n-doping), which increases electro-phonon scattering and weakens the vibration, whereas a blueshift corresponds to a lower electron concentration (p-doping), which weakens electro-phonon scattering and enhances the vibration.[41,46,53] In particular, 26DFBT functionalization resulted in a redshift of the A_{1g} peak of approximately 1.42 cm^{-1}, reflecting n-doping, whereas 35DFBT functionalization blueshifted by 1.17 cm^{-1}, suggesting p-doping. It is worth noting that the spectral resolution is ≈1.25 cm^{-1} (≈1 meV). The inset of Figure 3b depicts the dipole-induced doping effect and the dipole moment orientation of isomers grafted onto the MoS_2 monolayer, and the upward (downward) dipole orientation induces n-doping (p-doping), in agreement with the XPS results.

Figure 3c and d show the PL spectra and peak deconvolution analysis of monolayer MoS_2 before and after treatment. The PL spectra of monolayer MoS_2 exhibit two main peaks: the dominant A exciton peak at 1.85 eV and the relatively weak B exciton peak at 2.05 eV, which can be ascribed to the direct bandgap transition and spin−orbit splitting.[46] The reduced PL intensity of the d-MoS_2 was caused by the introduction of defects.[13,25] After 26DFBT functionalization, the peak intensity continues to decrease and redshift, while the intensity of MoS_2 functionalized with 35DFBT peak increased and blueshifted. This trend is in line with the dipole-induced change in the carrier density after functionalization of MoS_2 with the molecular isomers, which appears as a quenching and enhancement of the PL intensity resulting from n- and p-doping effects, respectively. Additionally, the A exciton peak can be deconvoluted into two components by Lorentz fitting, including a negative trion (X^-, red curve) peak at approximately 1.85 eV and a neutral exciton (X, blue curve) peak at around 1.89 eV, respectively. Both monolayer MoS_2 and d-MoS_2 containing defects exhibit a trion (X^-) peak that is more weighted than the neutral exciton (X) peak, though the X peak of d-MoS_2 is slightly enhanced. Following 26DFBT functionalization, the exciton peak X intensity decreased sharply, while the weight of the trion (X^-) peak increased, and the PL peak was dominated by the trion (X^-) peak, indicating a clear n-doping. In contrast, following 35DFBT functionalization, the weight of the neutral exciton (X) peak clearly increased, suggesting obvious p-doping. This result is similar to the electron/hole dopant-induced PL changes.[46,51,54]

To demonstrate the sensitivity of FETs based on monolayer MoS_2 for isomer identification, we performed electrical characterization of the devices before and after isomer functionalization (see the device schematic in Figure 1). Figure 4 shows the representative transfer (I_{ds} − V_{gs}) and output (I_{ds} − V_{ds}) characteristics of the FETs based on pristine monolayer MoS_2, after the introduction of defects and subsequent isomer functionalization. To monitor the modifications in the electrical characteristics of the devices upon isomer functionalization, as well as to avoid potential bias that may arise from the comparison of different devices, we compared changes based on the same device. We found that monolayer MoS_2 FETs exhibit typical n-type transport behavior (black curve). The introduction of defects (green curve) determines a subtle shift of the linear threshold voltage (V_{th}, see Figure S5 for the value extraction method) to negative gate voltages and a slight reduction of the on-state current (I_{on}). Such observations can be explained on the one hand in view of the introduction of S-defects acting as deep electron acceptors and on the other hand by the occurrence of p-doping originating from the oxidation of partial Mo atoms in the crystal.[42,44] However, the devices undergo opposite changes

https://doi.org/10.1021/acsnano.3c04194
ACS Nano 2023, 17, 17956−17965

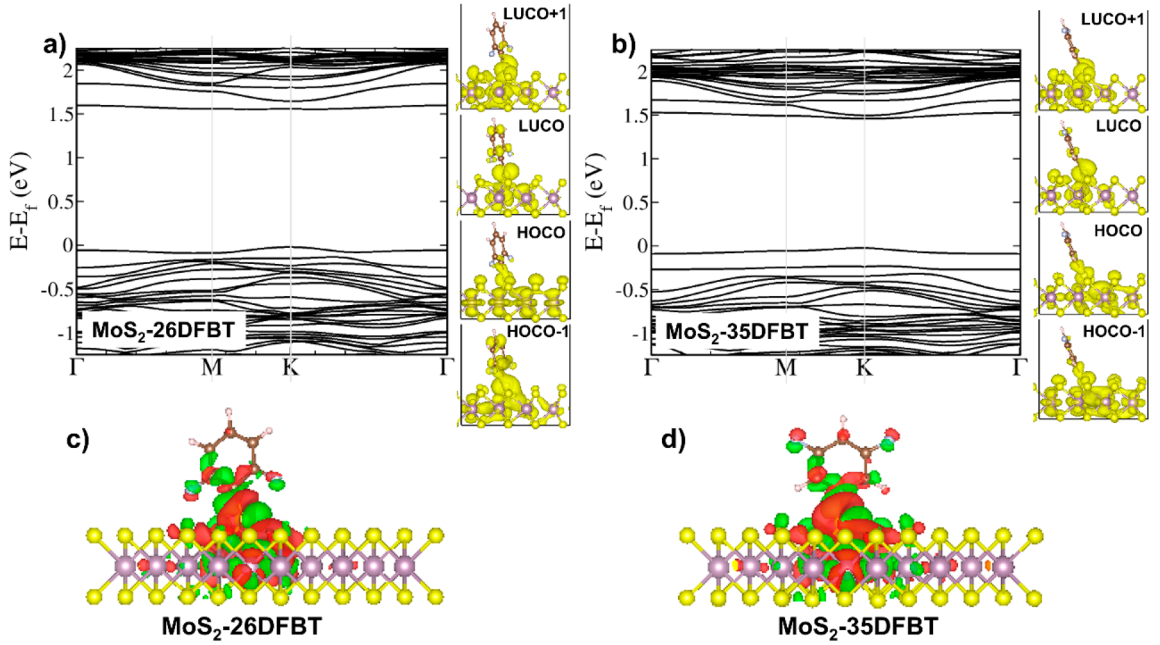

Figure 5. Electronic band structure of monolayer MoS_2 with the chemisorbed 26DFBT molecules (a) and 35DFBT molecules (b) on 3% S vacancy sites. The right panel shows the charge distribution of the highest occupied crystal orbital (HOCO and HOCO-1) and the lowest unoccupied crystal orbital (LUCO and LUCO-1). (c, d) Charge density difference maps of 26DFBT- and 35DFBT-functionalized monolayer MoS_2 on S vacancy sites, respectively, demonstrating a strong interaction between the isomers and MoS_2 (3% V_S).

following isomeric functionalization due to the doping effect induced by different dipole orientations of two molecules. 26DFBT-functionalized devices display a negative shift of the transfer curves (blue curve) and an increase of the I_{on}, indicating an n-doping effect. Conversely, 35DFBT-functionalized devices exhibit a positive shift of the transfer curves (red curve) and a decrease of the I_{on}, suggesting a p-doping effect. These findings are in agreement with previous XPS, Raman, and PL results. Furthermore, all devices exhibited I_{on}/I_{off} ratios exceeding 10^6 before and after functionalization, and the linear output curves demonstrate that all devices possess ohmic contact between the electrodes and the semiconductor, as evidenced in Figure 4c, which means that MoS_2 always maintains good semiconducting properties.

The changes in V_{th} and linear field-effect mobility (μ, see Experimental Section for the calculation method) of the devices before and after isomer functionalization can be obtained from the electrical curves. We counted dozens of devices and found that after functionalizing with 26DFBT, the V_{th} decreased by 20.3 ± 6.3 V, while the V_{th} increased by 18.8 ± 8.5 V after functionalizing with 35DFBT. The charge in the carrier density change (Δn) within the channel can be quantified by the change of V_{th} with the equation below:[40]

$$\Delta n = \frac{C_{ox}\Delta V_{th}}{e} = \frac{\varepsilon_{ox}\Delta V_{th}}{t_{ox}e} = 7.99 \times 10^{10}\Delta V_{th}\ \mathrm{cm}^{-2}$$

where C_{ox} is the capacitance per unit area of dielectric layer, ΔV_{th} is the change of V_{th}, e is the elementary charge, ε_{ox} is the dielectric constant of the dielectric layer, and t_{ox} is the thickness of dielectric layer. The value of Δn is indicative of the molecule's dipole-induced doping capability. Following the calculations, it was found that 26DFBT functionalization enables an increase in the carrier density by 1.62×10^{12} cm^{-2}, which in turn led to a 63.7% increase in mobility, while 35DFBT functionalization decreases the charge carrier density by 1.50×10^{12} cm^{-2}, which resulted in a 37.1% decrease in mobility. The amount of Δn in this study is comparable to the molecular dopants, indicating that device functionalization is an efficient and facile strategy for isomer identification.[41,46,54]

Furthermore, the detection capability of the device can be tuned by V_S on the MoS_2 surface. The V_S can be modulated by modifying the annealing time. Figure S6 and Table S2 show the XPS Mo 3d spectrum and calculated V_S as a function of annealing time. It can be seen that the V_S gradually increases with the increase of annealing time, which is consistent with previous results.[42] Figure 4f displays the ΔV_{th} of the devices before and after 26DFBT functionalization at different V_S (representative transfer curves are shown in Figure S7). They reveal that upon increasing V_S, the ΔV_{th} and the detection capability of the device gradually increase.

Theoretical calculations were performed to demonstrate the changes in MoS_2 before and after isomer functionalization. In particular, we calculated the dipole moment of the isolated molecules and the isomer-functionalized d-MoS_2 systems, as well as their work function (φ, WF) at the DFT/HSE06 level of theory; see Figure S8 and Table S3. For the sake of comparison, we extended the calculations to benzenethiol (BT), lacking any substituent on the aromatic ring, in order to best shed light on the changes induced by the fluorine substituents. Due to the different positions of the F atoms, 26DFBT features an upward dipole with a dipole moment (D_f) of −1.44 D, while 35DFBT shows a downward dipole with a D_f of +0.99 D. When chemically adsorbed on d-MoS_2 (3% V_S), the dipole moment direction of the isomer−MoS_2 systems is consistent with that of the isolated molecules, as evidenced in Figure S8d−f, and the WF changes accordingly: the WF calculated for MoS_2-26DFBT is lower than MoS_2-BT (5.14 eV) due to the upward dipole moment, while it is higher in MoS_2-35DFBT because of the downward dipole moment. Figure 5 displays the electronic band structure of monolayer MoS_2 chemisorbed with isomers on S vacancies (3% V_S) on a 4

https://doi.org/10.1021/acsnano.3c04194
ACS Nano 2023, 17, 17956−17965

× 4 × 1 supercell. The calculated φ of MoS_2-26DFBT and MoS_2-35DFBT are 5.09 and 5.42 eV, respectively. Compared to the d-MoS_2 (3% V_S) surface, with a φ of 5.23 eV, 26DFBT thus induces a relative n-doping with a 0.14 eV increase in WF, whereas 35DFBT induces a relative p-doping with a 0.19 eV decrease in WF. These relative shifts are consistent and in good quantitative agreement with the corresponding energy shifts measured by XPS. Also, the relative shift in the n-/p-doping due to functionalization is proportional to the axial dipole component of the molecule, similar to what is observed for WS_2 (3% V_S) and WSe_2 (3% V_{Se}) surfaces in our previous theoretical investigations.[55]

Figure 6 displays the scheme of the suggested mechanism of isomeric functionalization on the MoS_2 electronic structure.

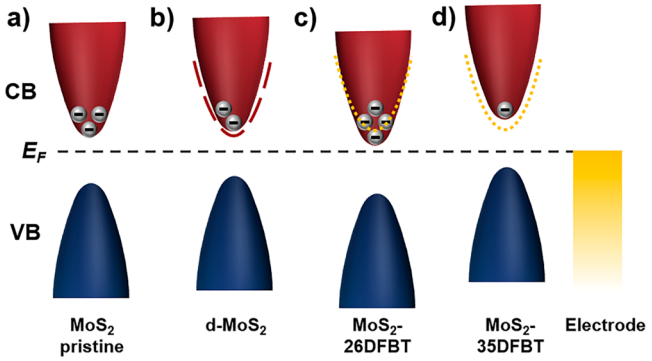

Figure 6. Mechanism of defect creation and isomer functionalization on the electronic structure of monolayer MoS_2. Fermi levels are aligned. The red and blue semiellipses denote the conduction band (CB) and valence band (VB), respectively. The red dashed line in (b) indicates the CB of pristine MoS_2. The yellow dotted lines in (c) and (d) indicate the CB of d-MoS_2.

Initially, mechanically exfoliated pristine monolayer MoS_2 crystals exhibit n-type semiconductor properties (Figure 6a). However, the introduction of S-defects serves as deep acceptors, which shift the Fermi energy level toward the VB, resulting in a reduction of the device performance (Figure 6b). Subsequently, upon isomer covalent functionalization, 26DFBT induces n-doping, which shifts the Fermi energy level toward the CB and enhances the device performance (Figure 6c), while 35DFBT induces p-doping, which shifts the Fermi energy level toward the VB and degrades the device performance (Figure 6d). Consequently, differences in the key performance indicators of the device can be used to differentiate between isomers.

A distinctive merit of our defect-engineering-based isomer identifier lies in its recyclable nature. The employed FET devices, upon completing isomer identification, can be subjected to elevated temperature annealing, thereby breaking the chemical bond and attaining the subsequent desorption of surface-bound isomeric entities. Notably, the sulfur moiety within the isomeric structure can heal the defects, thereby yielding the restoration of the device to its initial functional state (Figure S9, Supporting Information). Furthermore, we also tested the stability of isomer-functionalized FET devices. The transfer curves of the isomer-functionalized devices recorded after 1 week of storage in the glovebox (Figure S10, Supporting Information) revealed a good stability. In contrast, when stored in air, the device performance deteriorated with increasing storage time due to the well-known oxidation.

The strategy for discriminating isomers reported in this study stems from the extremely high sensitivity of defect-containing TMDCs to the environment in which even subtle changes in the surface can be manifested in their intrinsic properties, so that the functionalization of molecules with even small dipole moments can be recognized. Moreover, this recognition not only can be actualized within the confines of MoS_2 but also extends its purview to encompass other TMDCs as active material. As portrayed in Figure S11, when considering a monolayer of WSe_2 as the active medium, analogous outcomes are observed. This also illustrates the general applicability of the method. This manifestation concurrently underscores the overarching extensibility of the approach, thereby confirming its universal applicability.

CONCLUSIONS

In conclusion, this study demonstrates a universal method to identify isomers by introducing S-vacancy defects through defect engineering on mechanically exfoliated MoS_2 monolayers, followed by isomer functionalization via covalent grafting. The identification of isomers was accomplished by analyzing XPS data, Raman spectra, PL spectra, FET characteristics, and theoretical calculations. The distinct functionalization outcomes of MoS_2 monolayers resulted from the different magnitude and orientation of the dipoles in the molecular isomers, which led to discrepancies in the doping effects. These findings highlight the great potential of 2D materials for isomer identification and suggest that this approach could be a simple, efficient, and straightforward method for rapidly and selectively identifying isomers and other hardly distinguishable compounds.

EXPERIMENTAL INFORMATION

Materials. The MoS_2 and WSe_2 bulk crystal semiconductors were purchased from SPI. The 3,5-difluorobenzenethiol and 2,6-difluorobenzenethiol were purchased from Sigma-Aldrich.

Device Fabrication, Functionalization, and Characterization. TMDC monolayer flakes were mechanically exfoliated from a bulk crystal using Nitto adhesive tape, and then a PDMS film (purchased from Gel-Pak) was used to transfer the crystals from the tape on thermally oxidized silicon substrates covered with a 270-nm-thick SiO_2 layer as dielectrics (Fraunhofer Institute IPMS, $\rho_{Si} \approx 0.001$ Ω·cm) to minimize glue residue. Their thickness was monitored by optical microscopy combined with Raman spectroscopy and AFM. Back-gated FETs were fabricated by a conventional photolithography method, and the metal electrodes (0.2 nm Cr and 60 nm Au) were thermally evaporated onto the patterned substrate. Then a mild lift-off process was carried out in acetone (60 °C), and the as-prepared samples were annealed at 120 °C for 6 h in a high-vacuum chamber to improve the contacts and remove absorbents, such as water. During the defect creation process, as-prepared devices were treated on a hot plate at 300 °C for 1 h inside the glovebox to create S-defects in the channel. During the isomeric functionalization process, defects containing TMDC monolayer samples were immersed into a 1 mM DFBT in ethanol solution for 12 h, followed by rinsing with a large amount of ethanol and thermally annealed in a vacuum at 100 °C to remove surface physisorbed molecules, evaporate the solvent, and stabilize the system.

To effectuate the removal of isomer molecules from the crystal surface, an annealing procedure was conducted at 250 °C overnight within a high-vacuum environment.

The devices were electrically characterized by a Keithley dual-channel 2636A sourcemeter in a three-terminal configuration with the

https://doi.org/10.1021/acsnano.3c04194
ACS Nano 2023, 17, 17956−17965

back gate contacted through an underlying metal plate in a glovebox filled with nitrogen under dark conditions.

The linear carrier mobility μ was determined by the following equation:

$$\mu = \frac{dI_{ds}}{dV_{gs}} \times \frac{L}{WC_{ox}V_{ds}}$$

where L and W are the channel length and width and C_{ox} is the capacitance of the dielectric layer per unit area.

AFM Measurement. Tapping mode atomic force microscopy imaging was executed by means of a Bruker Dimension Icon setup operating in air. The tip model is TESPA-V2, and the tip stiffness K is 42 N m^{-1}. R_{RMS} from AFM topographical images was estimated on flake regions of 0.5 × 0.5 μm^2.

XPS Measurements. X-ray photoelectron spectroscopy measurements were carried out with a Thermo Scientific K-Alpha X-ray photoelectron spectrometer with a basic chamber pressure of $\approx 10^{-9}$ mbar and an Al anode as the X-ray source (X-ray radiation of 1486 eV). Spot sizes of 400 μm and pass energies of 200.00 eV for wide energy scans and 10.00−20.00 eV for scans were used. All XPS spectra were calibrated using the C 1s peak at 284.8 eV as a reference.

Raman and PL Spectroscopy. Raman and photoluminescence spectra were carried out in the atmosphere by a Renishaw inVia spectrometer equipped with a 532 nm laser. The excitation power was kept at no more than 1 mW to avoid local heating damage effects. The wavenumber (energy) resolution is about 1.25 cm^{-1} (≈1 meV).

Computational Details. DFT calculations were performed with the projector-augmented wave (PAW) basis set, as implemented in the VASP code.[56,57] Exchange and correlation effects were treated at the Perdew−Burke−Ernzerhof (PBE) level of theory and the dispersion forces by the Grimme correction (PBE+D2).[58,59] Dipole moment correction was employed along the 'c' axis (Z direction and perpendicular to the MoS_2 surface) with a kinetic energy cutoff of 600 eV and using a Monkhorst−Pack sampling of 3 × 3 × 1 for the Brillouin zone (BZ) integration on a 4 × 4 × 1 supercell of a MoS_2 monolayer with the vacuum space set to be 30 Å to avoid the interaction with periodic images. Geometries of pristine and defective (−3% V_S) MoS_2 surfaces, as well as the thiophenol adsorbed MoS_2-3% V_S, were fully optimized prior to calculation of work functions. The same computational criteria were used for calculations at the hybrid level of theory (HSE06). The work function (φ) of a (DF)BT-functionalized MoS_2 surface containing −3% sulfur vacancies (MoS_2-3% V_S) is calculated as the difference of Fermi energy (E_f) and the electrostatic potential at the vacuum level (E_p). The Fermi level (E_f) is set to the energy of the valence band maximum at the GGA/PBE level of theory and to the center of the electronic bandgap at the HSE06 level of theory.

ASSOCIATED CONTENT

Supporting Information

The Supporting Information is available free of charge at https://pubs.acs.org/doi/10.1021/acsnano.3c04194.

> Optical images and AFM morphology image of monolayer MoS_2, secondary-electron cutoff of isomer-functionalized Au substrate, Raman spectra of monolayer MoS_2 flake, calculation method of sulfur vacancy concentration, state-of-the-art comparison table, extraction method of threshold voltage (PDF)

AUTHOR INFORMATION

Corresponding Author

Paolo Samorì − *Université de Strasbourg, CNRS, ISIS UMR 7006, F-67000 Strasbourg, France*; Email: samori@unistra.fr

Authors

Bin Han − *Université de Strasbourg, CNRS, ISIS UMR 7006, F-67000 Strasbourg, France*

Sai Manoj Gali − *Université de Mons, Laboratory for Chemistry of Novel Materials, Mons 7000, Belgium*

Shuting Dai − *Université de Strasbourg, CNRS, ISIS UMR 7006, F-67000 Strasbourg, France; State Key Laboratory of Supramolecular Structure and Materials, College of Chemistry, Jilin University, Changchun 130012, China*

David Beljonne − *Université de Mons, Laboratory for Chemistry of Novel Materials, Mons 7000, Belgium*; orcid.org/0000-0002-2989-3557

Complete contact information is available at: https://pubs.acs.org/10.1021/acsnano.3c04194

Author Contributions

B.H. and P.S. conceived the experiments and designed the study. B.H. performed the AFM measurement, PL measurement, device fabrication, and characterization. S.D. and B.H. performed the optical characterization and electrical measurement. S.M.G. did the modeling work, under the supervision of D.B. All authors discussed the results and contributed to the interpretation of data. B.H. and P.S. cowrote the paper with input from all coauthors.

Notes

The authors declare no competing financial interest.

ACKNOWLEDGMENTS

This work was supported by the EC through the ERC project SUPRA2DMAT (GA-833707) and the Graphene Flagship Core 3 project (GA-881603) as well as the Labex project CSC (ANR-10LABX-0026 CSC) within the Investissement d'Avenir program ANR-10-IDEX-0002-02, the International Center for Frontier Research in Chemistry, the Institut Universitaire de France (IUF), and the Chinese Scholarship Council. The computational resources in Mons are supported by the FNRS "Consortium des Equipements de Calcul Intensif−CECI" program Grant No. 2.5020.11 and by the Walloon Region (ZENOBE Tier-1 supercomputer, under grant 1117545). S.M.G. is Chargé de Recherche−FNRS, and D.B. is Research Director−FNRS.

REFERENCES

(1) Manzeli, S.; Ovchinnikov, D.; Pasquier, D.; Yazyev, O. V.; Kis, A. 2D Transition Metal Dichalcogenides. *Nat. Rev. Mater.* **2017**, *2* (8), 17033.

(2) Wang, S.; Liu, X.; Xu, M.; Liu, L.; Yang, D.; Zhou, P. Two-Dimensional Devices and Integration Towards the Silicon Lines. *Nat. Mater.* **2022**, *21* (11), 1225−1239.

(3) Chhowalla, M.; Shin, H. S.; Eda, G.; Li, L.-J.; Loh, K. P.; Zhang, H. The Chemistry of Two-Dimensional Layered Transition Metal Dichalcogenide Nanosheets. *Nat. Chem.* **2013**, *5* (4), 263−275.

(4) Zhou, J.; Lin, J.; Huang, X.; Zhou, Y.; Chen, Y.; Xia, J.; Wang, H.; Xie, Y.; Yu, H.; Lei, J.; Wu, D.; Liu, F.; Fu, Q.; Zeng, Q.; Hsu, C.-H.; Yang, C.; Lu, L.; Yu, T.; Shen, Z.; Lin, H.; Yakobson, B. I.; Liu, Q.; Suenaga, K.; Liu, G.; Liu, Z. A Library of Atomically Thin Metal Chalcogenides. *Nature* **2018**, *556* (7701), 355−359.

(5) Radisavljevic, B.; Radenovic, A.; Brivio, J.; Giacometti, V.; Kis, A. Single-Layer MoS_2 Transistors. *Nat. Nanotechnol.* **2011**, *6* (3), 147−150.

(6) Wang, Q. H.; Kalantar-Zadeh, K.; Kis, A.; Coleman, J. N.; Strano, M. S. Electronics and Optoelectronics of Two-Dimensional Transition Metal Dichalcogenides. *Nat. Nanotechnol.* **2012**, *7* (11), 699−712.

(7) Mak, K. F.; He, K.; Lee, C.; Lee, G. H.; Hone, J.; Heinz, T. F.; Shan, J. Tightly Bound Trions in Monolayer MoS_2. *Nat. Mater.* **2013**, *12* (3), 207−211.
(8) Bian, Z.; Miao, J.; Zhao, Y.; Chai, Y. Strong Interlayer Interaction for Engineering Two-Dimensional Materials. *Acc. Mater. Res.* **2022**, *3* (12), 1220−1231.
(9) Liu, Y.; Weiss, N. O.; Duan, X.; Cheng, H.-C.; Huang, Y.; Duan, X. Van der Waals Heterostructures and Devices. *Nat. Rev. Mater.* **2016**, *1* (9), 16042.
(10) Zhao, Y.; Gobbi, M.; Hueso, L. E.; Samorì, P. Molecular Approach to Engineer Two-Dimensional Devices for CMOS and beyond-CMOS Applications. *Chem. Rev.* **2022**, *122* (1), 50−131.
(11) Bertolazzi, S.; Gobbi, M.; Zhao, Y.; Backes, C.; Samorì, P. Molecular Chemistry Approaches for Tuning the Properties of Two-Dimensional Transition Metal Dichalcogenides. *Chem. Soc. Rev.* **2018**, *47* (17), 6845−6888.
(12) Anichini, C.; Czepa, W.; Pakulski, D.; Aliprandi, A.; Ciesielski, A.; Samorì, P. Chemical Sensing with 2D Materials. *Chem. Soc. Rev.* **2018**, *47* (13), 4860−4908.
(13) Bertolazzi, S.; Bonacchi, S.; Nan, G.; Pershin, A.; Beljonne, D.; Samorì, P. Engineering Chemically Active Defects in Monolayer MoS_2 Transistors via Ion-Beam Irradiation and Their Healing via Vapor Deposition of Alkanethiols. *Adv. Mater.* **2017**, *29* (18), 1606760.
(14) Chen, X.; Berner, N. C.; Backes, C.; Duesberg, G. S.; McDonald, A. R. Functionalization of Two-Dimensional MoS_2: On the Reaction Between MoS_2 and Organic Thiols. *Angew. Chem., Int. Ed.* **2016**, *55* (19), 5803−5808.
(15) Bussolotti, F.; Yang, J.; Kawai, H.; Wong, C. P. Y.; Goh, K. E. J. Impact of S-Vacancies on the Charge Injection Barrier at the Electrical Contact with the MoS_2 Monolayer. *ACS Nano* **2021**, *15* (2), 2686−2697.
(16) Roy, S.; Choi, W.; Jeon, S.; Kim, D.-H.; Kim, H.; Yun, S. J.; Lee, Y.; Lee, J.; Kim, Y.-M.; Kim, J. Atomic Observation of Filling Vacancies in Monolayer Transition Metal Sulfides by Chemically Sourced Sulfur Atoms. *Nano Lett.* **2018**, *18* (7), 4523−4530.
(17) Xu, Y.; Wang, L.; Liu, X.; Zhang, S.; Liu, C.; Yan, D.; Zeng, Y.; Pei, Y.; Liu, Y.; Luo, S. Monolayer MoS_2 with S Vacancies from Interlayer Spacing Expanded Counterparts for Highly Efficient Electrochemical Hydrogen Production. *J. Mater. Chem. A* **2016**, *4* (42), 16524−16530.
(18) Yin, Y.; Han, J.; Zhang, Y.; Zhang, X.; Xu, P.; Yuan, Q.; Samad, L.; Wang, X.; Wang, Y.; Zhang, Z.; Zhang, P.; Cao, X.; Song, B.; Jin, S. Contributions of Phase, Sulfur Vacancies, and Edges to the Hydrogen Evolution Reaction Catalytic Activity of Porous Molybdenum Disulfide Nanosheets. *J. Am. Chem. Soc.* **2016**, *138* (25), 7965−7972.
(19) Chou, S. S.; De, M.; Kim, J.; Byun, S.; Dykstra, C.; Yu, J.; Huang, J.; Dravid, V. P. Ligand Conjugation of Chemically Exfoliated MoS_2. *J. Am. Chem. Soc.* **2013**, *135* (12), 4584−4587.
(20) Ippolito, S.; Kelly, A. G.; Furlan de Oliveira, R.; Stoeckel, M.-A.; Iglesias, D.; Roy, A.; Downing, C.; Bian, Z.; Lombardi, L.; Samad, Y. A.; Nicolosi, V.; Ferrari, A. C.; Coleman, J. N.; Samorì, P. Covalently Interconnected Transition Metal Dichalcogenide Networks via Defect Engineering for High-Performance Electronic Devices. *Nat. Nanotechnol.* **2021**, *16*, 592−598.
(21) Wang, Z.; Li, R.; Su, C.; Loh, K. P. Intercalated Phases of Transition Metal Dichalcogenides. *SmartMat* **2020**, *1* (1), No. e1013.
(22) Lin, Z.; Carvalho, B. R.; Kahn, E.; Lv, R.; Rao, R.; Terrones, H.; Pimenta, M. A.; Terrones, M. Defect Engineering of Two-Dimensional Transition Metal Dichalcogenides. *2D Materials* **2016**, *3* (2), 022002.
(23) Komsa, H.-P.; Krasheninnikov, A. V. Native Defects in Bulk and Monolayer MoS_2 from First Principles. *Phys. Rev. B* **2015**, *91* (12), 125304.
(24) Liu, D.; Chen, X.; Li, D.; Wang, F.; Luo, X.; Yang, B. Simulation of MoS_2 Crystal Structure and the Experimental Study of Thermal Decomposition. *J. Mol. Struct.* **2010**, *980* (1), 66−71.
(25) Mitterreiter, E.; Schuler, B.; Micevic, A.; Hernangómez-Pérez, D.; Barthelmi, K.; Cochrane, K. A.; Kiemle, J.; Sigger, F.; Klein, J.; Wong, E.; Barnard, E. S.; Watanabe, K.; Taniguchi, T.; Lorke, M.; Jahnke, F.; Finley, J. J.; Schwartzberg, A. M.; Qiu, D. Y.; Refaely-Abramson, S.; Holleitner, A. W.; Weber-Bargioni, A.; Kastl, C. The Role of Chalcogen Vacancies for Atomic Defect Emission in MoS_2. *Nat. Commun.* **2021**, *12* (1), 3822.
(26) Donarelli, M.; Bisti, F.; Perrozzi, F.; Ottaviano, L. Tunable Sulfur Desorption in Exfoliated MoS_2 by Means of Thermal Annealing in Ultra-High Vacuum. *Chem. Phys. Lett.* **2013**, *588*, 198−202.
(27) Mignuzzi, S.; Pollard, A. J.; Bonini, N.; Brennan, B.; Gilmore, I. S.; Pimenta, M. A.; Richards, D.; Roy, D. Effect of Disorder on Raman Scattering of Single-Layer MoS_2. *Phys. Rev. B* **2015**, *91* (19), 195411.
(28) Parkin, W. M.; Balan, A.; Liang, L.; Das, P. M.; Lamparski, M.; Naylor, C. H.; Rodríguez-Manzo, J. A.; Johnson, A. T. C.; Meunier, V.; Drndić, M. Raman Shifts in Electron-Irradiated Monolayer MoS_2. *ACS Nano* **2016**, *10* (4), 4134−4142.
(29) Giannazzo, F.; Fisichella, G.; Greco, G.; Di Franco, S.; Deretzis, I.; La Magna, A.; Bongiorno, C.; Nicotra, G.; Spinella, C.; Scopelliti, M.; Pignataro, B.; Agnello, S.; Roccaforte, F. Ambipolar MoS_2 Transistors by Nanoscale Tailoring of Schottky Barrier Using Oxygen Plasma Functionalization. *ACS Appl. Mater. Interfaces* **2017**, *9* (27), 23164−23174.
(30) Tosun, M.; Chan, L.; Amani, M.; Roy, T.; Ahn, G. H.; Taheri, P.; Carraro, C.; Ager, J. W.; Maboudian, R.; Javey, A. Air-Stable n-Doping of WSe_2 by Anion Vacancy Formation with Mild Plasma Treatment. *ACS Nano* **2016**, *10* (7), 6853−6860.
(31) Daukiya, L.; Seibel, J.; De Feyter, S. Chemical Modification of 2D Materials Using Molecules and Assemblies of Molecules. *Adv. Phys. X* **2019**, *4* (1), 1625723.
(32) Hu, Z.; Wu, Z.; Han, C.; He, J.; Ni, Z.; Chen, W. Two-Dimensional Transition Metal Dichalcogenides: Interface and Defect Engineering. *Chem. Soc. Rev.* **2018**, *47* (9), 3100−3128.
(33) Brill, A. R.; Koren, E.; de Ruiter, G. Molecular Functionalization of 2D Materials: from Atomically Planar 2D Architectures to Off-Plane 3D Functional Materials. *J. Mater. Chem. C* **2021**, *9* (35), 11569−11587.
(34) Makarova, M.; Okawa, Y.; Aono, M. Selective Adsorption of Thiol Molecules at Sulfur Vacancies on MoS_2(0001), Followed by Vacancy Repair via S-C Dissociation. *J. Phys. Chem. C* **2012**, *116* (42), 22411−22416.
(35) Wang, B.; Huynh, T. P.; Wu, W.; Hayek, N.; Do, T. T.; Cancilla, J. C.; Torrecilla, J. S.; Nahid, M. M.; Colwell, J. M.; Gazit, O. M.; Puniredd, S. R.; McNeill, C. R.; Sonar, P.; Haick, H. A Highly Sensitive Diketopyrrolopyrrole-Based Ambipolar Transistor for Selective Detection and Discrimination of Xylene Isomers. *Adv. Mater.* **2016**, *28* (21), 4012−4018.
(36) Li, H.; Zhang, Q.; Yap, C. C. R.; Tay, B. K.; Edwin, T. H. T.; Olivier, A.; Baillargeat, D. From Bulk to Monolayer MoS_2: Evolution of Raman Scattering. *Adv. Funct. Mater.* **2012**, *22* (7), 1385−1390.
(37) Zhao, Y.; Ippolito, S.; Samorì, P. Functionalization of 2D Materials with Photosensitive Molecules: From Light-Responsive Hybrid Systems to Multifunctional Devices. *Adv. Opt. Mater.* **2019**, *7* (16), 1900286.
(38) Gobbi, M.; Orgiu, E.; Samorì, P. When 2D Materials Meet Molecules: Opportunities and Challenges of Hybrid Organic/Inorganic van der Waals Heterostructures. *Adv. Mater.* **2018**, *30* (18), 1706103.
(39) Liu, Y.; Guo, J.; Zhu, E.; Liao, L.; Lee, S.-J.; Ding, M.; Shakir, I.; Gambin, V.; Huang, Y.; Duan, X. Approaching the Schottky-Mott Limit in Van der Waals Metal-Semiconductor Junctions. *Nature* **2018**, *557* (7707), 696−700.
(40) Han, B.; Zhao, Y.; Ma, C.; Wang, C.; Tian, X.; Wang, Y.; Hu, W.; Samorì, P. Asymmetric Chemical Functionalization of Top-Contact Electrodes: Tuning the Charge Injection for High-Performance MoS_2 Field-Effect Transistors and Schottky Diodes. *Adv. Mater.* **2022**, *34* (12), 2109445.
(41) Wang, Y.; Gali, S. M.; Slassi, A.; Beljonne, D.; Samorì, P. Collective Dipole-Dominated Doping of Monolayer MoS_2: Orientation and Magnitude Control via the Supramolecular Approach. *Adv. Funct. Mater.* **2020**, *30* (36), 2002846.

https://doi.org/10.1021/acsnano.3c04194
ACS Nano 2023, 17, 17956−17965

(42) Sim, D. M.; Kim, M.; Yim, S.; Choi, M.-J.; Choi, J.; Yoo, S.; Jung, Y. S. Controlled Doping of Vacancy-Containing Few-Layer MoS_2 via Highly Stable Thiol-Based Molecular Chemisorption. *ACS Nano* **2015**, *9* (12), 12115−12123.
(43) Gao, L.; Liao, Q.; Zhang, X.; Liu, X.; Gu, L.; Liu, B.; Du, J.; Ou, Y.; Xiao, J.; Kang, Z.; Zhang, Z.; Zhang, Y. Defect-Engineered Atomically Thin MoS_2 Homogeneous Electronics for Logic Inverters. *Adv. Mater.* **2020**, *32* (2), 1906646.
(44) Grünleitner, T.; Henning, A.; Bissolo, M.; Zengerle, M.; Gregoratti, L.; Amati, M.; Zeller, P.; Eichhorn, J.; Stier, A. V.; Holleitner, A. W.; Finley, J. J.; Sharp, I. D. Real-Time Investigation of Sulfur Vacancy Generation and Passivation in Monolayer Molybdenum Disulfide via in situ X-ray Photoelectron Spectromicroscopy. *ACS Nano* **2022**, *16* (12), 20364−20375.
(45) Nan, H.; Wang, Z.; Wang, W.; Liang, Z.; Lu, Y.; Chen, Q.; He, D.; Tan, P.; Miao, F.; Wang, X.; Wang, J.; Ni, Z. Strong Photoluminescence Enhancement of MoS_2 through Defect Engineering and Oxygen Bonding. *ACS Nano* **2014**, *8* (6), 5738−5745.
(46) Zhang, S.; Hill, H. M.; Moudgil, K.; Richter, C. A.; Hight Walker, A. R.; Barlow, S.; Marder, S. R.; Hacker, C. A.; Pookpanratana, S. J. Controllable, Wide-Ranging n-Doping and p-Doping of Monolayer Group 6 Transition-Metal Disulfides and Diselenides. *Adv. Mater.* **2018**, *30* (36), 1802991.
(47) Vericat, C.; Vela, M. E.; Benitez, G.; Carro, P.; Salvarezza, R. C. Self-Assembled Monolayers of Thiols and Dithiols on Gold: New Challenges for A Well-Known System. *Chem. Soc. Rev.* **2010**, *39* (5), 1805−1834.
(48) Han, B.; Li, Y.; Ji, X.; Song, X.; Ding, S.; Li, B.; Khalid, H.; Zhang, Y.; Xu, X.; Tian, L.; Dong, H.; Yu, X.; Hu, W. Systematic Modulation of Charge Transport in Molecular Devices through Facile Control of Molecule-Electrode Coupling Using a Double Self-Assembled Monolayer Nanowire Junction. *J. Am. Chem. Soc.* **2020**, *142* (21), 9708−9717.
(49) Zhao, Y.; Gali, S. M.; Wang, C.; Pershin, A.; Slassi, A.; Beljonne, D.; Samorì, P. Molecular Functionalization of Chemically Active Defects in WSe_2 for Enhanced Opto-Electronics. *Adv. Funct. Mater.* **2020**, *30* (45), 2005045.
(50) Foerster, A.; Gemming, S.; Seifert, G.; Tomanek, D. Chemical and Electronic Repair Mechanism of Defects in MoS_2 Monolayers. *ACS Nano* **2017**, *11* (10), 9989−9996.
(51) Mouri, S.; Miyauchi, Y.; Matsuda, K. Tunable Photoluminescence of Monolayer MoS_2 via Chemical Doping. *Nano Lett.* **2013**, *13* (12), 5944−5948.
(52) Wu, J.; Li, H.; Yin, Z.; Li, H.; Liu, J.; Cao, X.; Zhang, Q.; Zhang, H. Layer Thinning and Etching of Mechanically Exfoliated MoS_2 Nanosheets by Thermal Annealing in Air. *Small* **2013**, *9* (19), 3314−3319.
(53) Li, Y.; Xu, C.-Y.; Hu, P.; Zhen, L. Carrier Control of MoS_2 Nanoflakes by Functional Self-Assembled Monolayers. *ACS Nano* **2013**, *7* (9), 7795−7804.
(54) Kang, D.-H.; Kim, M.-S.; Shim, J.; Jeon, J.; Park, H.-Y.; Jung, W.-S.; Yu, H.-Y.; Pang, C.-H.; Lee, S.; Park, J.-H. High-Performance Transition Metal Dichalcogenide Photodetectors Enhanced by Self-Assembled Monolayer Doping. *Adv. Funct. Mater.* **2015**, *25* (27), 4219−4227.
(55) Gali, S. M.; Beljonne, D. Combined Healing and Doping of Transition Metal Dichalcogenides Through Molecular Functionalization. *J. Mater. Chem. C* **2021**, *9* (45), 16247−16256.
(56) Kresse, G.; Furthmüller, J. Efficient Iterative Schemes for ab Initio Total-Energy Calculations Using a Plane-Wave Basis Set. *Phys. Rev. B* **1996**, *54* (16), 11169−11186.
(57) Kresse, G.; Joubert, D. From Ultrasoft Pseudopotentials to The Projector Augmented-Wave Method. *Phys. Rev. B* **1999**, *59* (3), 1758−1775.
(58) Perdew, J. P.; Burke, K.; Ernzerhof, M. Generalized Gradient Approximation Made Simple. *Phys. Rev. Lett.* **1996**, *77* (18), 3865−3868.
(59) Grimme, S. Semiempirical GGA-type density functional constructed with a long-range dispersion correction. *J. Comput. Chem.* **2006**, *27* (15), 1787−1799.

https://doi.org/10.1021/acsnano.3c04194
ACS Nano 2023, 17, 17956−17965